Coordinate Independence of the Schwarzschild Black Hole Accretion Vlasov Gas Model*

Ping Li (李平)[1,2†] Jun Cheng (程俊)[1,2‡] Jiang-he Yang (杨江河)[1,3§]

[1]College of Mathematics and Physics, Hunan University of Arts and Sciences, 3150 Dongting Dadao, Changde City, Hunan Province 415000, China
[2]Hunan Province Key Laboratory Integration of Photoelectric Information Integration and Optical Manufacturing Technology, 3150 Dongting Dadao, Changde City, Hunan Province 415000, China
[3]Center for Astrophysics, Guangzhou University, 230 West Ring Road, Guangzhou, Guangdong Province 510006, China

Abstract: This paper presents a detailed study of the coordinate dependence of Vlasov gas accretion onto a Schwarzschild black hole. Asymptotic results at infinity and near the horizon are obtained using Taylor expansions for three different statistical distributions within the framework of the most general stationary, spherically symmetric spacetime. Our findings demonstrate that the particle number density, energy density, radial and tangential pressures, and accretion rates are independent of the coordinate choice, although individual components, such as the particle current density and the stress-energy tensor, explicitly depend on the coordinate system. Consequently, the accretion theory can be formulated without reference to any particular coordinate system. We also show that the mean energy of the accreted particles is $m_0 + k_B T$, which is lower than the mean energy $m_0 + \frac{3}{2}k_B T$ of the Maxwell-Boltzmann system in the classical limit. The specific entropy of the accreted particles is also lower than the global average by $\frac{3}{2}k_B$. This difference arises because lower-energy particles are more easily accreted, whereas higher-energy particles are more readily scattered. We also present numerical results at finite radii for the relevant physical quantities.

DOI: 10.1088/1674-1137/aebd70 **CSTR:**

CPC Accepted

I. INTRODUCTION

The problem of stationary, spherically symmetric accretion of matter onto a black hole has a long history, dating back to the classical work of Bondi [1] and Michel [2] in the hydrodynamic regime. In these seminal studies, the gas was modeled as a perfect fluid, and explicit solutions for the mass accretion rate were obtained under the assumption of a polytropic equation of state. However, in high-temperature, low-density astrophysical environments, such as those observed around the supermassive black holes at the centers of the Galaxy (Sgr A*) and M87 [3, 4], the mean free path of particles can greatly exceed the characteristic system scale, rendering collisional effects negligible. In such collisionless or weakly collisional plasmas, the hydrodynamic description breaks down, and a kinetic approach based on the Vlasov equation becomes essential. The formal structure of relativistic kinetic theory on curved spacetimes has been developed over decades, with foundational contributions by Synge [5], Ehlers [6], and, more recently, Sarbach and Zannias [7–9], who provided a rigorous geometric framework for formulating the Vlasov equation on the tangent and cotangent bundles. For a comprehensive review of the Einstein–Vlasov system, see Andréasson [10].

In 2017, Rioseco and Sarbach provided the first systematic study of the accretion of a relativistic, collisionless kinetic gas (the Vlasov gas) onto a Schwarzschild black hole [11, 12]. Working within the Hamiltonian formulation on the cotangent bundle, they solved the relativistic Liouville equation, derived the most general solution for the distribution function in terms of action-angle variables, and computed the associated observables, including the particle current density and stress–energy–momentum tensor. In the steady-state, spherically symmetric case with an equilibrium distribution at infinity, they found that, in the low-temperature limit, the tangential pressure at the horizon is about an order of mag-

Received 29 July 2026; Accepted 4 November 2026

* This work was supported in part by the National Natural Science Foundation of China (Grant No. 12505071) and the Research Foundation of the Education Bureau of Hunan Province, China (Grant No. 25B0635). It was also supported in part by the Key Laboratory of Information Detection and Intelligent Processing Technology of the Hunan Provincial Department of Education and by the Applied Characteristic Subject of Hunan Province, "Electronic Science and Technology".

† E-mail: Lip57120@huas.edu.cn
‡ E-mail: chengjun@huas.edu.cn
§ E-mail: yjianghe@163.com

©2026 Chinese Physical Society and the Institute of High Energy Physics of the Chinese Academy of Sciences and the Institute of Modern Physics of the Chinese Academy of Sciences and IOP Publishing Ltd. All rights, including for text and data mining, AI training, and similar technologies, are reserved.

nitude larger than the radial pressure. This result explicitly demonstrates that a collisionless gas behaves very differently from an isotropic perfect fluid. It also provided a partial explanation for the known fact that the kinetic accretion rate is much lower than that in the hydrodynamic Bondi–Michel case [1, 2]. Moreover, they established the asymptotic stability of steady-state spherical flows by proving pointwise convergence results for a broad class of initial conditions [12]. The accretion of a Vlasov gas onto a Schwarzschild black hole was also studied from the perspective of geodesic motion and analytic solutions for timelike and null geodesics by Cieślik and Mach [13, 14].

The Rioseco–Sarbach model has since been extended to a variety of spherically symmetric black hole spacetimes. Mach and Odrzywołek derived exact axially symmetric solutions for accretion onto a moving Schwarzschild black hole [15, 16], providing a relativistic counterpart of the Bondi–Hoyle–Lyttleton problem, and further extended this work to the low-temperature limit and numerical aspects [17]. Cieślik and Mach generalized the analysis to Reissner–Nordström black holes [18], showing that the mass accretion rate decreases with increasing black hole charge. Li, Yang, and Xu later studied the accretion of a degenerate Fermi gas using Fermi–Dirac statistics [19], demonstrating the effect of quantum statistics on the accretion process in a charged background. Liu and Zhang provided a complete analytical treatment of two-component plasma Vlasov gas accretion onto a Reissner–Nordström black hole [20], addressing the electromagnetic interactions between charged particles. Gamboa et al. considered a generalization of the Bondi-type model in which the boundary conditions are specified at a sphere of finite radius instead of at infinity [21], highlighting the role of angular momentum in the accretion flow. The model was further extended to regular black holes, such as the Bardeen black hole [22], and to Schwarzschild-like black holes in modified gravity theories, such as bumblebee gravity [23]. Momennia and Sarbach recently provided a general framework for spherical accretion of a collisionless kinetic gas into generic static, asymptotically flat black hole spacetimes [24]. Zhang and Jiang investigated Vlasov gas accretion onto a black hole in the Kalb–Ramond field [25]. In parallel, axisymmetric stationary collisionless gas configurations surrounding Schwarzschild black holes were analyzed by Gabarrete and Sarbach [26, 27], and Shapiro studied spikes and accretion of unbound collisionless matter around black holes [28].

The extension of the Vlasov gas accretion model to rotating black hole spacetimes has proven considerably more challenging because of the loss of spherical symmetry and the complexity of the Kerr geodesic structure. Mach, Momennia, and Sarbach established a complete accretion theory for a Vlasov gas in Kerr spacetime [29, 30], providing a rigorous phase-space characterization of absorption and scattering orbits and deriving analytic slow-rotation approximations that accurately describe the accretion process even for rapidly rotating black holes. Li, Liu, and Zhai also provided integral expressions for the particle current density and stress–energy tensor in full (3+1)-dimensional Kerr spacetime and numerically computed the accretion rate per unit solid angle [31]. Liu extended the analysis to Kerr–Newman spacetime and studied plasma Vlasov gas accretion under a weak electromagnetic coupling approximation [32]. Finite collisionless accretion disks in Kerr spacetime were constructed by Khan and Mach [33], and stable collisionless tori around Kerr black holes were investigated by Luepker, Yuan, and Chen [34]. The relaxation of macroscopic variables to a stationary state around a Kerr black hole due to phase-space mixing was studied by Rioseco and Sarbach [35, 36]. The general properties of timelike and null geodesics in Kerr spacetime, which are essential for the phase-space analysis of kinetic accretion, have been studied by Cieślik, Hackmann, and Mach [14] and by Tejeda, Taylor, and Miller [37]; a recent analysis in horizon-penetrating coordinates was given by Bakun et al. [38]. Hydrodynamical accretion onto rotating black holes has also been studied numerically by Aguayo-Ortiz et al. [39], providing a complementary perspective to the kinetic approach. The slow-rotation approximation for Kerr black holes, which is astrophysically relevant, was further analyzed by Pani, Berti, and Gualtieri in the context of gravitational perturbations [40]. An exact hydrodynamical solution for Bondi-type accretion onto a Kerr black hole was obtained by Petrich, Shapiro, and Teukolsky for an ultra-hard equation of state [41].

Monte Carlo methods have been developed for stationary solutions of general-relativistic Vlasov systems [42, 43], providing an alternative numerical approach that complements analytical studies. These methods are particularly useful for handling complex phase-space geometries and validating analytical approximations in regimes where direct numerical integration becomes challenging.

Despite these advances, two fundamental aspects of Vlasov gas accretion theory have not been fully clarified. First, the coordinate dependence of the formalism has not been systematically investigated. Although individual components of the particle current density and the stress–energy tensor explicitly depend on the choice of coordinate system, physical observables such as the particle number density, energy density, and pressures should be coordinate-independent. Nevertheless, previous studies have typically been formulated in specific coordinate systems —such as Eddington–Finkelstein or Painlevé–Gullstrand coordinates—and a general proof of the invariance of all relevant physical quantities has been lacking. Second, the thermodynamic properties of the

CPC Accepted

particles that are actually captured by the black hole—as opposed to those scattered back to infinity —have not been examined in detail. In particular, it remains unclear how the angular-momentum filtering mechanism, which distinguishes absorbed from scattered trajectories, affects the mean energy and entropy of the accreted particles, and how this compares with the classical Maxwell–Boltzmann expectation.

In this paper, we address both of these open questions. We perform our calculations within the framework of the most general stationary, spherically symmetric spacetime. This framework allows us to consider different coordinate representations simultaneously — including orthogonal Schwarzschild coordinates, Eddington–Finkelstein coordinates, and Painlevé–Gullstrand-type coordinates—and to demonstrate explicitly that the accretion theory can be formulated without reference to any particular coordinate system. We show that although the components J_μ and $T_{\mu\nu}$ depend on the coordinate choice, the eigenvalues of the mixed stress–energy tensor $T^\mu{}_\nu$ (which give the energy density ρ, radial pressure $p_{\rm rad}$, and tangential pressure $p_{\rm tan}$) and the particle number density $n = \sqrt{-g_{\mu\nu}J^\mu J^\nu}$ are coordinate-invariant scalars. Furthermore, we prove that the particle and energy accretion rates $\dot{n}$ and $\dot{E}$, defined via the conserved currents associated with the Killing symmetries, are also coordinate-independent, with the identity $a^2b^2+h^2=1$ ensuring that the formulas take the simple forms $-4\pi r^2 J^r$ and $-4\pi r^2 T^r{}_t$ in all coordinates considered. We also examine the thermodynamic properties of the accreted particles for three different quantum statistics: Fermi–Dirac, Maxwell–Jüttner, and Bose–Einstein. In the classical limit, we find that the mean energy of the particles captured by the black hole is $m_0 + k_B T$, which is lower than the mean energy $m_0 + \frac{3}{2}k_B T$ of the Maxwell–Jüttner gas at infinity. This reduction arises because high-energy particles tend to carry large angular momenta, making them more likely to be scattered by the centrifugal barrier. Consequently, the specific entropy of the accreted particles is lower than the global average by $\frac{3}{2}k_B$. Our results demonstrate that the accretion theory can be formulated in a coordinate-invariant manner and that the angular-momentum selection effect has important consequences for the thermodynamic evolution of the black hole–gas system.

The paper is organized as follows. In Sec. II, we present the general metric for a stationary, spherically symmetric spacetime and derive the equations of motion for test particles. In Sec. III, we construct the action-angle variables that trivialize the Liouville equation. In Sec. IV, we introduce the relativistic equilibrium distributions for three different quantum statistics: Fermi–Dirac, Maxwell–Jüttner, and Bose–Einstein. In Sec. V, we derive the integral expressions for the particle current density and the stress–energy–momentum tensor. In Sec. VI, we discuss the limits of integration and the classification of absorption and scattering orbits. In Sec. VII, we identify the coordinate-independent physical quantities and discuss the diagonalization of the stress–energy tensor. In Secs. VIII and IX, we analyze the asymptotic behavior at infinity and near the horizon, respectively. In Sec. X, we specialize to the Maxwell–Jüttner distribution and derive the accretion rates of thermodynamic quantities. In Sec. XI, we present numerical results for finite radii. Finally, Sec. XII contains our conclusions and discussion.

II. EQUATIONS OF MOTION FOR TEST PARTICLES IN A GENERAL SPHERICALLY SYMMETRIC STATIONARY SPACETIME

In this paper, we consider a general spherically symmetric, stationary spacetime with the metric

$$ds^2 = -b^2(r)dt^2 - 2h(r)dtdr + a^2(r)dr^2 + r^2 d\theta^2 + r^2\sin^2\theta d\varphi^2, \tag{1}$$

where $b(r)$, $h(r)$, and $a(r)$ are arbitrary functions of the radial coordinate r. This form includes a non-diagonal component, $g_{tr} = -h(r)$. Therefore, ∂_t is a timelike Killing vector; however, because $g_{tr} \neq 0$, this Killing vector is not orthogonal to the hypersurfaces $t = \text{constant}$, and the spacetime is stationary but not static. The determinant of the metric is $\det(g) = -r^4\sin^2\theta(a^2b^2+h^2)$, and the inverse metric can be written in matrix form as

$$g^{\mu\nu} = \begin{pmatrix} -\dfrac{a^2}{a^2b^2+h^2} & -\dfrac{h}{a^2b^2+h^2} & 0 & 0 \\ -\dfrac{h}{a^2b^2+h^2} & \dfrac{b^2}{a^2b^2+h^2} & 0 & 0 \\ 0 & 0 & \dfrac{1}{r^2} & 0 \\ 0 & 0 & 0 & \dfrac{1}{r^2\sin^2\theta} \end{pmatrix}. \tag{2}$$

The metric form (1) allows us to study the influence of different coordinate choices on the accretion theory. For instance, in the case of an orthogonal spacetime, the Schwarzschild black hole is described by the standard form

$$b^2(r) = a^{-2}(r) = 1 - \frac{2M}{r}, \qquad h(r) = 0.$$

Alternatively, one may adopt Eddington–Finkelstein coordinates by introducing the transformation

$$u = t + \int^r \left(\frac{1}{b^2(r')} - \eta(r')\right) dr',$$

The metric in Eq. (1) can be transformed into

CPC Accepted

$$ds^2 = -b^2du^2 + 2(1-b^2\eta)dudr + \eta(2-b^2\eta)dr^2 + r^2(d\theta^2 + \sin^2\theta d\phi^2),$$

where $b^2 = 1-2M/r$, $a^2 = \eta(2-b^2\eta)$, and $h = 1-b^2\eta$. In this work, we focus on three specific cases: the orthogonal (static) Schwarzschild coordinates ($h=0$), the Eddington-Finkelstein form with $h=1$ (or $\eta=0$), and the case $h=2M/r$ (or $\eta=1$). The case $h=2M/r$ has been extensively discussed in the literature. For the Schwarzschild metric, it can be shown that

$$a^2b^2 + h^2 = 1. \tag{3}$$

Moreover, by employing the general metric (1), our results can be readily extended to Reissner-Nordström black holes and even to asymptotically flat black holes in modified theories of gravity.

Consider a test particle of mass m moving in this background. Its dynamics is described by the Lagrangian

$$\mathcal{L} = \frac{1}{2}g_{\mu\nu}\frac{dx^\mu}{d\lambda}\frac{dx^\nu}{d\lambda}, \tag{4}$$

where λ denotes an affine parameter. Substituting the metric (1) into (4) yields

$$\mathcal{L} = -\frac{1}{2}b(r)^2\dot{t}^2 - h(r)\dot{t}\dot{r} + \frac{1}{2}a(r)^2\dot{r}^2 + \frac{1}{2}r^2\dot{\theta}^2 + \frac{1}{2}r^2\sin^2\theta\dot{\phi}^2, \tag{5}$$

where the dot denotes differentiation with respect to λ. The canonical momenta obtained from the Lagrangian are:

$$p_t = \frac{\partial\mathcal{L}}{\partial\dot{t}} = -b^2(r)\dot{t} - h(r)\dot{r}, \tag{6}$$

$$p_r = \frac{\partial\mathcal{L}}{\partial\dot{r}} = -h(r)\dot{t} + a(r)^2\dot{r}, \tag{7}$$

$$p_\theta = \frac{\partial\mathcal{L}}{\partial\dot{\theta}} = r^2\dot{\theta}, \tag{8}$$

$$p_\phi = \frac{\partial\mathcal{L}}{\partial\dot{\phi}} = r^2\sin^2\theta\dot{\phi}. \tag{9}$$

Because the metric is independent of t and ϕ, the corresponding canonical momenta are conserved. We define the particle's energy E and angular momentum l_z as

$$E \equiv -p_t = b^2(r)\dot{t} + h(r)\dot{r}, \tag{10}$$

$$l_z \equiv p_\phi = r^2\sin^2\theta\dot{\phi}. \tag{11}$$

Spherical symmetry also ensures the conservation of the squared total angular momentum, l^2. The Hamiltonian, obtained by a Legendre transformation, is

$$H = p_\mu\dot{x}^\mu - \mathcal{L} = \frac{1}{2}g_{\mu\nu}\dot{x}^\mu\dot{x}^\nu, \tag{12}$$

and its conservation yields the rest-mass constraint

$$m^2 = -2H = -g_{\mu\nu}\dot{x}^\mu\dot{x}^\nu. \tag{13}$$

To derive the radial equation of motion, we solve for $\dot{t}$ and $\dot{r}$ from (10) and (7). Written in matrix form, these equations are

$$\begin{pmatrix} b^2(r) & h(r) \\ h(r) & -a^2(r) \end{pmatrix}\begin{pmatrix} \dot{t} \\ \dot{r} \end{pmatrix} = \begin{pmatrix} E \\ -p_r \end{pmatrix}, \tag{14}$$

we find

$$\dot{t} = \frac{a^2(r)E + h(r)p_r}{a^2(r)b^2(r) + h^2(r)}, \tag{15}$$

$$\dot{r} = \frac{-h(r)E - b^2(r)p_r}{a^2(r)b^2(r) + h^2(r)}. \tag{16}$$

Substituting (15) and (16) into the mass constraint (13), and using (11) together with the expression for p_θ, we obtain, after simplification, an effective one-dimensional equation for the radial motion. In terms of the conserved quantities,

$$\dot{r}^2 = \frac{1}{a^2(r)b^2(r) + h^2(r)}\left[E^2 - m^2b^2(r) - \frac{b^2(r)l^2}{r^2}\right], \tag{17}$$

where $l^2 = p_\theta^2 + p_\phi^2/\sin^2\theta$ denotes the square of the total angular momentum. To simplify subsequent calculations, we introduce the notation

$$R \equiv r^4\dot{r}^2 = \frac{r^4}{a^2b^2 + h^2}\left[E^2 - b^2\left(m^2 + \frac{l^2}{r^2}\right)\right]. \tag{18}$$

This term represents the effective kinetic energy associated with radial motion.

III. ACTION-ANGLE VARIABLES

In this section, we construct the action-angle variables for a neutral test particle moving in the general sta-

CPC Accepted

tionary, spherically symmetric spacetime described by the metric (1). The cyclic coordinates t and ϕ allow us to separate the Hamilton–Jacobi equation and introduce conserved quantities that serve as the new momenta. The action-angle variables then provide a convenient framework for solving the Vlasov equation.

The abbreviated action, or Hamilton's characteristic function, along a particle orbit is defined as

$$S = \int p_t dt + \int p_r dr + \int p_\theta d\theta + \int p_\phi d\phi, \tag{19}$$

where the integral is taken along the trajectory. The use of the characteristic function to analyze geodesic motion and connect it with observable quantities in black hole spacetimes has been discussed in various contexts [49, 50]. The four conserved quantities are p_t, p_ϕ, l^2, and m^2. Substituting $p_t = -E$ and $p_\phi = l_z$ into the mass constraint gives

$$m^2 = -g^{tt}E^2 + 2g^{tr}Ep_r - g^{rr}p_r^2 - \frac{l^2}{r^2}. \tag{20}$$

Substituting the components of the inverse metric (2) and solving the resulting quadratic equation for p_r yields

$$p_r = -\frac{hE}{b^2} \pm \frac{\sqrt{a^2b^2+h^2}}{b^2}\sqrt{E^2 - b^2\left(m^2 + \frac{l^2}{r^2}\right)} \equiv -\frac{hE}{b^2} \pm \frac{(a^2b^2+h^2)\sqrt{R}}{b^2r^2}. \tag{21}$$

The two signs correspond to the outgoing and incoming branches of the radial motion. For the angular component, we obtain

$$p_\theta = \pm\sqrt{l^2 - \frac{l_z^2}{\sin^2\theta}}. \tag{22}$$

Thus, the abbreviated action in (19) can be written as

$$S = -Et + l_z\phi + \int p_r\, dr + \int p_\theta\, d\theta, \tag{23}$$

where the radial and angular integrals are evaluated along the orbit. The action is a function of the coordinates (t,ϕ,r,θ) and the constants (E,l_z,l,m). Because the system is completely integrable, we can perform a canonical transformation to new variables (Q^μ, P_μ), for which the new momenta are precisely these constants:

$$P_0 = m, \quad P_1 = E, \quad P_2 = l_z, \quad P_3 = l. \tag{24}$$

The new coordinates (i.e., the angle variables) are defined by

$$Q^\mu = \frac{\partial S}{\partial P_\mu}, \qquad \mu = 0,1,2,3. \tag{25}$$

Using the previously defined quantity R (see Eq. (18)) to simplify the radial integrals, the angular variables are expressed as follows:

$$Q^0 = \frac{\partial S}{\partial m} = -m\int \frac{r^2}{\sqrt{R}}dr, \tag{26}$$

$$Q^1 = \frac{\partial S}{\partial E} = -t + \int\left(-\frac{h}{b^2} \pm \frac{Er^2}{b^2\sqrt{R}}\right)dr, \tag{27}$$

$$Q^2 = \frac{\partial S}{\partial l_z} = \phi - l_z\int \frac{d\theta}{\sin^2\theta\sqrt{l^2 - \sin^{-2}\theta\, l_z^2}}, \tag{28}$$

$$Q^3 = \frac{\partial S}{\partial l} = -l\int\frac{1}{\sqrt{R}}dr + l\int\frac{d\theta}{\sqrt{l^2 - \sin^{-2}\theta\, l_z^2}}. \tag{29}$$

These expressions define the action-angle variables (Q^μ, P_μ).

In these variables the Hamiltonian depends only on the new momenta, namely $H = \frac{1}{2}P_0^2$. Consequently the Vlasov equation $\{f,H\} = 0$ for the distribution function f reduces, after the canonical transformation, to

$$\frac{\partial f}{\partial Q^0} = 0, \tag{30}$$

since H does not depend on Q^0. By stationarity and spherical symmetry, f is also independent of Q^1, Q^2, Q^3, P_2. Thus f can be taken as an arbitrary function of the conserved quantities alone [11]

$$f = f(P_0, P_1, P_3). \tag{31}$$

This result is essential for constructing steady-state accretion flows: we may choose a distribution function that describes a thermal equilibrium at infinity and then compute the particle current density and the stress-energy tensor by integrating over momentum space.

IV. RELATIVISTIC EQUILIBRIUM DISTRIBUTIONS

We assume that the gas surrounding the black hole is in local thermodynamic equilibrium at infinity and the natural choice for the equilibrium distribution is [44]

CPC Accepted

$$f_\infty = A\frac{1}{\exp[(E-\mu)/k_BT]+\varepsilon}, \tag{32}$$

where A is a normalisation constant, k_B is Boltzmann's constant, T is the temperature, and μ is the chemical potential. The parameter ε distinguishes three different types of quantum statistics

- $\varepsilon = +1$: **Fermi–Dirac statistics**. This describes a gas of fermions (half-integer spin particles) that obey the Pauli exclusion principle. At most one particle can occupy a given quantum state. Examples include electrons, protons, and neutrons. The distribution is essential for describing degenerate matter such as that found in white dwarfs and neutron stars.
- $\varepsilon = 0$: **Maxwell–Jüttner statistics** [45, 46]. This is the relativistic generalisation of the classical Maxwell–Boltzmann distribution. It is valid when quantum effects are negligible, i.e., when the particle density is low or the temperature is high enough that the occupation numbers are small ($\exp[(E-\mu)/k_BT] \gg 1$).
- $\varepsilon = -1$: **Bose–Einstein statistics**. This describes a gas of bosons (integer spin particles). In contrast to fermions, any number of bosons can occupy the same quantum state. Photons in a blackbody cavity and certain dark matter candidates are typical examples.

To simplify the calculation of observable quantities, we consider a gas composed of identical test particles, all having the same rest mass m_0. It is convenient to incorporate this constraint directly into the distribution function by including a delta function $\delta(P_0 - m_0)$ that selects only those particles with the correct mass, where the delta function does not affect the validity of the Vlasov equation. The resulting distribution function remains a solution of the Vlasov equation throughout the spacetime. Therefore, we adopt the following full distribution function:

$$f = \delta(P_0 - m_0)A\frac{1}{\exp[(P_1-\mu)/k_BT]+\varepsilon}, \tag{33}$$

where $P_0 = m$ and $P_1 = E$. At infinity, integration over the mass variable using the delta function recovers the original equilibrium distribution f_∞. This choice greatly simplifies the phase-space integrals in the computation of the particle current density and the stress-energy tensor, as will be shown in the following sections.

It is important to note that while the functional form (33) is used everywhere, the physical interpretation of T and μ as the temperature and chemical potential is strictly valid only at infinity. In the vicinity of the black hole, these parameters serve merely as convenient labels that characterise the ensemble; the local thermodynamic equilibrium is not necessarily maintained because the gas is collisionless. Nevertheless, the distribution (33) provides a steady-state, spherically symmetric solution of the relativistic Vlasov equation that is consistent with the asymptotic thermal bath. This approach has been widely adopted in the literature on relativistic kinetic accretion.

Although the Vlasov gas is collisionless and does not maintain local thermodynamic equilibrium near the black hole, redshifted thermodynamic scalars can still be defined that remain finite and coordinate-invariant across the horizon. For a static observer in the Schwarzschild geometry, Tolman's and Klein's laws give

$$T(r)\sqrt{-g_{tt}(r)} = T_\infty, \qquad \mu(r)\sqrt{-g_{tt}(r)} = \mu_\infty, \tag{34}$$

with $g_{tt} = -(1-2M/r)$. Since $\sqrt{-g_{tt}} \to 0$ as $r \to r_H$, the local quantities $T(r)$ and $\mu(r)$ diverge at the horizon, whereas the redshifted combinations T_∞, μ_∞ and the ratio $\mu/T = \mu_\infty/T_\infty$ remain finite and constant. These redshifted scalars thus provide the coordinate-invariant observables in terms of which the thermodynamic interpretation is consistently formulated up to the horizon, in direct analogy with the coordinate independence of $\dot{n}$ established in this work. For the collisionless Vlasov gas, however, they should be regarded as formally defined scalar observables rather than genuine local thermodynamic variables, since no local equilibrium is established near the horizon.

V. THE PARTICLE CURRENT DENSITY AND THE STRESS ENERGY-MOMENTUM TENSOR

The particle current density and the stress-energy-momentum tensor are defined as

$$J_\mu = \int p_\mu f(x,p)\,\mathrm{dvol}_x(p), \tag{35}$$

$$T_{\mu\nu} = \int p_\mu p_\nu f(x,p)\,\mathrm{dvol}_x(p), \tag{36}$$

with the invariant phase-space volume element

$$\mathrm{dvol}_x(p) = \sqrt{-\det(g^{\mu\nu})}\,d^4p = \sqrt{-\det(g^{\mu\nu})}\,dp_t\,dp_r\,dp_\theta\,dp_\phi, \tag{37}$$

where $\sqrt{-\det(g^{\mu\nu})} = \dfrac{1}{r^2\sin\theta\sqrt{a^2b^2+h^2}}$. The covariant momenta in terms of the conserved quantities are gaven by Eqs. (21) and (22). We further introduce

$$p_\theta = l\cos\sigma, \tag{38}$$

$$p_\phi = l\sin\theta\sin\sigma, \tag{39}$$

CPC Accepted

and change variables from $(p_t, p_r, p_\theta, p_\phi)$ to (m^2, E, l_z, l^2) and then to (E, l, σ). The Jacobian of the first transformation is

$$\frac{\partial(m^2, E, l_z, l^2)}{\partial(p_t, p_r, p_\theta, p_\phi)} = 4(g^{rr}p_r + g^{tr}p_t)p_\theta. \tag{40}$$

The second transformation gives

$$dl_z\, dl^2 = 2l^2 \sin\theta \cos\sigma\, dl\, d\sigma. \tag{41}$$

Combining these with $\sqrt{-\det(g^{\mu\nu})}$, we obtain after canceling $\cos\sigma$ the volume element

$$\mathrm{dvol}_x(p) = \frac{ml}{\sqrt{R}}\, dm\, dE\, dl\, d\sigma. \tag{42}$$

We now perform the σ integrals. Using the identities

$$\int_0^{2\pi} \sin\sigma\, d\sigma = \int_0^{2\pi} \cos\sigma\, d\sigma = \int_0^{2\pi} \sin\sigma\cos\sigma\, d\sigma = 0, \tag{43}$$

and

$$\int_0^{2\pi} \sin^2\sigma\, d\sigma = \int_0^{2\pi} \cos^2\sigma\, d\sigma = \pi, \tag{44}$$

we find that the following components vanish: $J_\theta, J_\phi, T_{t\theta}, T_{t\phi}$ (linear in $\cos\sigma$ or $\sin\sigma$) and $T_{\theta\phi}$ (proportional to $\sin\sigma\cos\sigma$). And for the angular diagonal components we obtain $T_{\theta\theta} = \dfrac{T_{\phi\phi}}{\sin^2\theta}$. The remaining non-zero components after the σ integration are:

$$J_t = -2\pi m_0 A \iint \frac{El}{\sqrt{R_0}} \frac{1}{\exp[(E-\mu)/k_BT] + \varepsilon} dE\, dl, \tag{45}$$

$$J_r = 2\pi m_0 A \iint \frac{l}{b^2}\left(\pm\frac{a^2b^2 + h^2}{r^2} - \frac{hE}{\sqrt{R_0}}\right) \times \frac{1}{\exp[(E-\mu)/k_BT] + \varepsilon} dE\, dl, \tag{46}$$

$$T_{tt} = 2\pi m_0 A \iint \frac{E^2 l}{\sqrt{R_0}} \frac{1}{\exp[(E-\mu)/k_BT] + \varepsilon} dE\, dl, \tag{47}$$

$$T_{tr} = -2\pi m_0 A \iint \frac{El}{b^2}\left(\pm\frac{a^2b^2 + h^2}{r^2} - \frac{hE}{\sqrt{R_0}}\right) \times \frac{1}{\exp[(E-\mu)/k_BT] + \varepsilon} dE\, dl, \tag{48}$$

$$T_{rr} = 2\pi m_0 A \iint \frac{l\sqrt{R_0}}{b^4}\left(\pm\frac{a^2b^2 + h^2}{r^2} - \frac{hE}{\sqrt{R_0}}\right)^2 \frac{1}{\exp[(E-\mu)/k_BT] + \varepsilon} dE\, dl, \tag{49}$$

$$T_{\theta\theta} = \pi m_0 A \iint \frac{l^3}{\sqrt{R_0}} \frac{1}{\exp[(E-\mu)/k_BT] + \varepsilon} dE\, dl, \tag{50}$$

where R_0 is the function R in the case of $m = m_0$. For the absorption part, there is only the branch "+"; and for the scarring part, there are both the branches "+" and "-". In the above expression, the r component depends particularly on the choice of coordinates. This explicit coordinate dependence will be analyzed in the following sections.

VI. THE LIMITS OF INTEGRATION

In this section, we will discuss the integral limits of Eqs. (45) - (50). For the Schwarzschild black hole we have $b^2 = 1 - 2M/r$ and the identity $a^2b^2 + h^2 = 1$ holds in all coordinate systems. Specializing the general radial equation (17) to a particle of mass m_0 gives

$$R = (E^2 - m_0^2)r^4 + 2Mm_0^2 r^3 - l^2(r^2 - 2Mr). \tag{51}$$

There are three categories for those particles incident from infinity: those that fall into the black hole and are absorbed, those that are scattered by the black hole and return to infinity, and—lying between these two scenarios—a critical case in which particles neither enter the black hole nor escape to infinity, but instead asymptotically approach an unstable bound orbit. The critical orbits satisfy $R = 0$ and $\partial_r R = 0$, Solving them yields the well-known expression (see e.g. Ref. [47])

$$l_c^2(E) = \frac{M^2}{2} \frac{27E^4 - 36E^2m_0^2 + 8m_0^4 + E(9E^2 - 8m_0^2)^{3/2}}{E^2 - m_0^2}, \tag{52}$$

which determined the critical momentum $l = l_c(E)$. Thus, the quantities J_μ and $T_{\mu\nu}$ are naturally separate into three parts: the absorbed, the scattered, and the critical parts, which are [47]

$$J_\mu = J_\mu^{\mathrm{abs}} + J_\mu^{\mathrm{scat}} + J_\mu^{\mathrm{cri}}, \tag{53}$$

$$T_{\mu\nu} = T_{\mu\nu}^{\mathrm{abs}} + T_{\mu\nu}^{\mathrm{scat}} + T_{\mu\nu}^{\mathrm{cri}}. \tag{54}$$

Particles are captured if $l < l_c(E)$ and scattered if

CPC Accepted

$l > l_c(E)$. It is worth emphasizing that the critical orbit $l = l_c(E)$ corresponds to a measure-zero set in phase space and therefore contributes nothing to the integrals for J_μ and $T_{\mu\nu}$. At fixed $m = m_0$ the integration domain is three-dimensional in (E, l, σ). Since the condition $l = l_c(E)$ does not involve σ, for each E it selects a one-dimensional set along σ, and as E varies these sets sweep out a two-dimensional surface embedded in the three-dimensional domain, which has zero three-dimensional measure. Geometrically, $l = l_c(E)$ is a separatrix: it separates the absorbed region $l < l_c(E)$ from the scattered region $l > l_c(E)$, but it belongs to neither, and a boundary has no measure. Consequently $\int_{l_c}^{l_c} f(l)\,\mathrm{d}l = 0$ and the critical parts vanish identically, $J_\mu^{\rm crit} = T_{\mu\nu}^{\rm crit} = 0$. The critical orbit also satisfies the parametric relations

$$l_c^2 = \frac{M r_c^2 m_0^2}{r_c - 3M}, \qquad E = m_0 \frac{r_c - 2M}{\sqrt{r_c(r_c - 3M)}}, \tag{55}$$

where r_c is the unstable circular orbit. For the photon orbit, this value is $r_c = 3M$.

For a scattered particle to reach a given radius r, the energy must be at least the value obtained by interpreting r as the critical radius r_c in (55):

$$E_{\min}(r) = m_0 \frac{r - 2M}{\sqrt{r(r - 3M)}}, \qquad r > 3M. \tag{56}$$

This expression diverges as $r \to 3M^+$, equals m_0 at $r = 4M$, and approaches m_0 from above as $r \to \infty$. Since a particle coming from infinity must satisfy $E \geq m_0$, the expression is valid only for $3M < r < 4M$; for $r > 4M$ the minimal energy is m_0, while for $r < 3M$ no scattered particle can reach that radius ($E_{\min} = \infty$). Hence

$$E_{\min}(r) = \begin{cases} \infty, & r < 3M, \\ m_0 \dfrac{r - 2M}{\sqrt{r(r - 3M)}}, & 3M \leq r \leq 4M, \\ m_0, & r > 4M. \end{cases} \tag{57}$$

The maximal angular momentum at given E and r follows from (51) with $\dot{r}^2 \geq 0$:

$$l_{\max}^2(E, r) = r^2 \left(\frac{E^2}{1 - 2M/r} - m_0^2 \right). \tag{58}$$

Using the general expressions (51) for the particle current and stress-energy tensor, the absorption and scattering contributions are obtained by restricting the integrals as follows:

- **Absorption:** $E \in [m_0, \infty)$, $l \in [0, l_c(E))$.
- **Scattering:** $E \in [E_{\min}(r), \infty)$, $l \in (l_c(E), l_{\max}(E, r)]$.

The total quantities are the sum of absorption and scattering parts.

VII. COORDINATE-INDEPENDENT PHYSICAL QUANTITIES

The particle current density J_μ and stress-energy tensor $T_{\mu\nu}$ depend on the choice of coordinates through the metric functions $a(r), b(r), h(r)$. However, certain combinations of their components are invariant under coordinate transformations that preserve spherical symmetry and stationarity. In this section we identify these invariants: the eigenvalues of $T^\mu{}_\nu$ (giving the energy density and pressures) and the particle number density derived from J^μ. We also clarify the coordinate independence of accretion rates. Throughout this section we use the fact that the metric (1) satisfies the identity $a^2 b^2 + h^2 = 1$, which holds for all coordinate choices considered in this paper.

A. Diagonalisation of the stress-energy tensor

The mixed tensor $T^\mu{}_\nu = g^{\mu\rho} T_{\rho\nu}$ has the block-diagonal form

$$T^\mu{}_\nu = \begin{pmatrix} T^t{}_t & T^t{}_r & 0 & 0 \\ T^r{}_t & T^r{}_r & 0 & 0 \\ 0 & 0 & T^\theta{}_\theta & 0 \\ 0 & 0 & 0 & T^\phi{}_\phi \end{pmatrix}, \qquad T^\phi{}_\phi = T^\theta{}_\theta. \tag{59}$$

The eigenvalues of the (t, r) block are

$$\lambda_\pm = \frac{T^t{}_t + T^r{}_r \pm \sqrt{(T^t{}_t - T^r{}_r)^2 + 4 T^t{}_r T^r{}_t}}{2}. \tag{60}$$

The energy density $\rho > 0$ is the negative of the negative eigenvalue, and the radial pressure $p_{\rm rad}$ is the positive eigenvalue:

$$\rho = -\lambda_- = \frac{1}{2}\left(-T^t{}_t - T^r{}_r + \sqrt{(T^t{}_t - T^r{}_r)^2 + 4 T^t{}_r T^r{}_t} \right), \tag{61}$$

$$p_{\rm rad} = \lambda_+ = \frac{1}{2}\left(T^t{}_t + T^r{}_r + \sqrt{(T^t{}_t - T^r{}_r)^2 + 4 T^t{}_r T^r{}_t} \right). \tag{62}$$

The tangential pressure is simply

$$p_{\rm tan} = T^\theta{}_\theta = \frac{T_{\theta\theta}}{r^2}. \tag{63}$$

These three scalars $\rho, p_{\rm rad}, p_{\rm tan}$ are coordinate-inde-

CPC Accepted

pendent, as they are eigenvalues of a tensor.

For a perfect fluid at rest, the stress-energy tensor would be diagonal with $p_{\rm rad} = p_{\tan} = p$. In the Vlasov gas, however, one generally finds $p_{\rm rad} \neq p_{\tan}$ in the finite radii. This indicates that the Vlasov gas is an anisotropic fluid. Following Letelier [48], the stress-energy tensor can be decomposed into a sum of a perfect fluid (with pressure $p_{\tan}$) and a null fluid that carries a radial energy flux

$$T^{\mu\nu} = T^{\mu\nu}_{\rm perfect} + T^{\mu\nu}_{\rm null}. \tag{64}$$

The null component is responsible for the off-diagonal entries $T^{t}{}_{r}$ and $T^{r}{}_{t}$.

B. Particle number density and accretion rates

The particle number density is defined as

$$n = \sqrt{-g_{\mu\nu}J^{\mu}J^{\nu}}. \tag{65}$$

This quantity is a scalar and therefore coordinate-independent, even though the individual components J^{μ} and the metric depend on the coordinate choice.

For a steady, spherically symmetric flow, the conservation law $\nabla_{\mu}J^{\mu} = 0$ reduces to

$$\frac{\partial}{\partial r}\left(r^2 J^{r}\right) = 0, \tag{66}$$

where we have used the identity $a^2b^2 + h^2 = 1$ which implies $\sqrt{-g} = r^2\sin\theta$. Hence the quantity

$$\dot{n} \equiv -4\pi r^2 J^{r} \tag{67}$$

is constant with respect to r. Evaluating this constant at the event horizon r_{+} gives the particle accretion rate (number of particles crossing the horizon per unit time). Despite the fact that J^{r} itself depends on the coordinate system, the product $-4\pi r^2 J^{r}$ is invariant because the transformation properties of J^{r} exactly compensate the change in the area element.

Similarly, the energy accretion rate is defined using the conserved current associated with the timelike Killing vector ∂_t. The stress-energy conservation $\nabla_{\mu}T^{\mu}_{t} = 0$ leads to

$$\frac{\partial}{\partial r}\left(r^2 T^{r}_{t}\right) = 0, \tag{68}$$

so that

$$\dot{E} \equiv -4\pi r^2 T^{r}_{t} \tag{69}$$

is also constant and coordinate-independent. For a gas of identical neutral particles of mass m_0, the mass accretion rate is simply

$$\dot{M} = m_0\dot{n}. \tag{70}$$

These accretion rates are the primary physical quantities that determine how the black hole's mass evolves over time.

In summary, while the components J^{μ} and $T^{\mu\nu}$ depend on the coordinate system, the derived scalars n, ρ, $p_{\rm rad}$, $p_{\tan}$ and the integrated rates $\dot{n}$, $\dot{E}$ are invariant. The identity $a^2b^2 + h^2 = 1$ ensures that the formulas for the accretion rates take the simple form $-4\pi r^2 J^{r}$ and $-4\pi r^2 T^{r}_{t}$ in all coordinates considered, while the underlying physical quantities remain unchanged.

VIII. ASYMPTOTIC BEHAVIOR AT INFINITY

In this section we study the asymptotic behavior of the particle current density J_{μ} and the stress-energy tensor $T_{\mu\nu}$ in the limit $r \to \infty$. Only the scattering part contributes; the absorption part vanishes at large distances. We use the general metric of Sec. II, which satisfies $a^2b^2 + h^2 = 1$, and specialize to the Schwarzschild black hole with $b^2 = 1 - 2M/r$. The radial kinetic term for a particle of mass m_0 is rewritten as

$$R_0 = r^4\dot{r}^2 = X - Yl^2, \qquad X = r^4\left(E^2 - b^2 m_0^2\right), \quad Y = r^2 b^2. \tag{71}$$

For $r \to \infty$ the integration domain simplifies to

$$E \in [m_0, \infty), \qquad l \in [l_c(E), l_{\max}(E, r)], \quad l_{\max} = \sqrt{X/Y}.$$

The critical angular momentum $l_c(E)$ is independent of r and is given by Eq. (52). We also define $R_{0c} = X - Yl_c^2$.

We next expand the relevant quantities in powers of $1/r$. For a Schwarzschild black hole,

$$b^2(r) = 1 - \frac{2M}{r}, \tag{72}$$

$$h(r) = h_0 + \frac{h_1}{r} + \cdots, \tag{73}$$

$$a^2(r) = 1 - h_0^2 + \frac{2M(1 - h_0^2) - 2h_0h_1}{r} + \cdots, \tag{74}$$

where h_0 and h_1 depend on the choice of coordinates. Defining $\Delta = E^2 - m_0^2$, we obtain the following integrals:

CPC Accepted

$$I_1 \equiv \int_{l_c}^{l_{\max}} l\,dl = \frac{1}{2}\left(\frac{X}{Y} - l_c^2\right) = r^2\left(\frac{\Delta}{2} + \frac{M}{r}(m_0^2+\Delta) + O\left(\frac{1}{r^2}\right)\right), \tag{75}$$

$$I_2 \equiv \int_{l_c}^{l_{\max}} \frac{l}{\sqrt{R_0}}\,dl = \frac{\sqrt{R_{0c}}}{Y} = \sqrt{\Delta} + \frac{M}{r}\frac{m_0^2+2\Delta}{\sqrt{\Delta}} + O\left(\frac{1}{r^2}\right), \tag{76}$$

$$I_3 \equiv \int_{l_c}^{l_{\max}} \frac{l^3}{\sqrt{R_0}}\,dl = \frac{\sqrt{R_{0c}}}{3Y^2}\left(2A + Bl_c^2\right) = \frac{2r^2}{3}\left(\Delta^{3/2} + \frac{M\sqrt{\Delta}}{r}(3m_0^2+4\Delta) + O\left(\frac{1}{r^2}\right)\right), \tag{77}$$

$$I_4 \equiv \int_{l_c}^{l_{\max}} l\sqrt{R_0}\,dl = \frac{R_{0c}^{3/2}}{3Y} = \frac{r^4}{3}\left(\Delta^{3/2} + \frac{M\sqrt{\Delta}}{r}(3m_0^2+2\Delta) + O\left(\frac{1}{r^2}\right)\right). \tag{78}$$

Substituting these expansions into the integrals (45)–(50) and defining the average $\langle Q(E)\rangle = \int_{m_0}^{\infty} \frac{Q(E)}{\exp[(E-\mu)/k_BT]+\varepsilon}\,dE$, we obtain the following asymptotic results.

a. Coordinate-independent components:

$$J_t^{\infty} = -4\pi A m_0\left[\langle\sqrt{\Delta}E\rangle + \frac{M}{r}\langle E\left(\frac{m_0^2}{\sqrt{\Delta}} + 2\sqrt{\Delta}\right)\rangle + O\left(\frac{1}{r^2}\right)\right], \tag{79}$$

$$T_{tt}^{\infty} = 4\pi A m_0\left[\langle\sqrt{\Delta}E^2\rangle + \frac{M}{r}\langle E^2\left(\frac{m_0^2}{\sqrt{\Delta}} + 2\sqrt{\Delta}\right)\rangle + O\left(\frac{1}{r^2}\right)\right], \tag{80}$$

$$T_{\theta\theta}^{\infty} = \frac{4\pi r^2}{3} A m_0\left[\langle\Delta^{3/2}\rangle + \frac{M}{r}\langle\sqrt{\Delta}(3m_0^2+4\Delta)\rangle + O\left(\frac{1}{r^2}\right)\right]. \tag{81}$$

b. Coordinate-dependent components:

$$J_r^{\infty} = -4\pi A m_0\left(h_0\langle E\sqrt{\Delta}\rangle + \frac{1}{r}\langle\frac{E}{\sqrt{\Delta}}(h_0 M(m_0^2+4\Delta)+h_1\Delta)\rangle + O\left(\frac{1}{r^2}\right)\right), \tag{82}$$

$$T_{tr}^{\infty} = 4\pi A m_0\left(h_0\langle E^2\sqrt{\Delta}\rangle + \frac{1}{r}\langle\frac{E^2}{\sqrt{\Delta}}(h_0 M(m_0^2+4\Delta)+h_1\Delta)\rangle + O\left(\frac{1}{r^2}\right)\right), \tag{83}$$

$$T_{rr}^{\infty} = \frac{4}{3}\pi A m_0\left(\langle\Delta^{3/2}\rangle + 3h_0^2\langle E^2\sqrt{\Delta}\rangle + \frac{3}{r}\langle\frac{M\Delta(m_0^2+2\Delta)+E^2h_0(Mh_0(m_0^2+6\Delta)+2h_1\Delta)}{\sqrt{\Delta}}\rangle + O\left(\frac{1}{r^2}\right)\right). \tag{84}$$

We now compute the particle number density $n_{\infty} = \sqrt{-g_{\mu\nu}J_{\infty}^{\mu}J_{\infty}^{\nu}}$. Using the contravariant components $J^{\mu} = g^{\mu\nu}J_{\nu}$ and the leading constant parts of J_t and J_r from Eqs. (79) and (82), together with the inverse metric components to order r^0,

$$g^{tt} = -(1-h_0^2), \quad g^{tr} = -h_0, \quad g^{rr} = 1,$$

we obtain

$$n_{\infty} = \sqrt{-g^{tt}(J_t)^2 - 2g^{tr}J_tJ_r - g^{rr}(J_r)^2} = 4\pi A m_0\langle\sqrt{\Delta}E\rangle. \tag{85}$$

All dependence on h_0 and h_1 disappears, confirming that the particle number density is a coordinate scalar.

We then compute the mixed tensor $T^{\infty\mu}{}_{\nu} = g^{\mu\rho}T_{\rho\nu}^{\infty}$ to leading order. Using the constant parts of the covariant components, we obtain

$$T^{\infty t}{}_{t} = g^{tt}T_{tt}^{\infty} + g^{tr}T_{rt}^{\infty} = -4\pi A m_0\langle\sqrt{\Delta}E^2\rangle, \tag{86}$$

$$T^{\infty r}{}_{r} = g^{rr}T_{rr}^{\infty} + g^{tr}T_{tr}^{\infty} = \frac{4}{3}\pi A m_0\langle\Delta^{3/2}\rangle, \tag{87}$$

$$T^{\infty t}{}_{r} = g^{tt}T_{tr}^{\infty} + g^{tr}T_{rr}^{\infty} = -4\pi A m_0 h_0\left(\langle E^2\sqrt{\Delta}\rangle + \frac{1}{3}\langle\Delta^{3/2}\rangle\right), \tag{88}$$

$$T^{\infty r}{}_{t} = g^{rr}T_{rt}^{\infty} + g^{tr}T_{tt}^{\infty} = 0. \tag{89}$$

Thus, the (t,r)-block of $T^{\infty\mu}{}_{\nu}$ is upper triangular; therefore, the energy density $\rho^{\infty} = -T^{\infty t}{}_{t}$ and the radial pressure $p_{\mathrm{rad}}^{\infty} = T^{\infty r}{}_{r}$ are

CPC Accepted

$$\rho^{\infty} = 4\pi A m_0 \langle \sqrt{\Delta} E^2 \rangle, \tag{90}$$

$$p^{\infty}_{\mathrm{rad}} = \frac{4}{3}\pi A m_0 \langle \Delta^{3/2} \rangle. \tag{91}$$

The tangential pressure is obtained from the angular component:

$$p^{\infty}_{\tan} = \frac{T^{\infty}_{\theta\theta}}{r^2} = \frac{4}{3}\pi A m_0 \langle \Delta^{3/2} \rangle = p^{\infty}_{\mathrm{rad}}. \tag{92}$$

Thus, at infinity, the Vlasov gas is isotropic, and the pressure satisfies the equation of state for a relativistic ideal gas. Moreover, all expressions are manifestly independent of h_0 and h_1, confirming their coordinate invariance.

IX. BEHAVIOR NEAR THE EVENT HORIZON

We now investigate the behavior of the particle current density and stress–energy tensor near the event horizon, $r = 2M$. It is convenient to introduce the small parameter

$$x \equiv r - 2M, \tag{93}$$

and expand the metric functions $b^2(r)$, $h(r)$, and $a^2(r)$ as power series in x. Using the identity $a^2 b^2 + h^2 = 1$, we obtain

$$b^2(r) = \frac{x}{2M} - \frac{x^2}{4M^2} + O(x^3), \tag{94}$$

$$h(r) = H_0 + H_1 x + O(x^2), \tag{95}$$

$$a^2(r) = \frac{2M(1-H_0^2)}{x} + 1 - H_0^2 - 4H_0 H_1 M + O(x), \tag{96}$$

where H_0 and H_1 are constants that specify the coordinate choice. For the Schwarzschild black hole, the auxiliary functions X and Y, defined in Eq. (71), become

$$X = 16M^4E^2 + 8M^3(4E^2 - m_0^2)\,x + O(x^2),$$
$$Y = 2Mx + x^2 + O(x^3). \tag{97}$$

Near the event horizon $r = 2M$, only the absorption component contributes. Therefore, the integration interval for the angular momentum is $l \in [0, l_c(E)]$, where $l_c(E)$ is given by Eq. (52) and is independent of x. The radial momentum corresponds to the incoming branch (the minus sign in p_r). The integrals I_1–I_4 in Eqs. (75)–(78) can be evaluated in closed form over the interval $[0, l_c]$. Expanding the results in powers of x yields

$$\mathcal{I}_1 \equiv \int_0^{l_c} l\,dl = \frac{l_c^2}{2}, \tag{98}$$

$$\mathcal{I}_2 \equiv \int_0^{l_c} \frac{l}{\sqrt{R_0}}\,dl = \frac{\sqrt{X} - \sqrt{R_{0c}}}{Y}$$
$$= \frac{l_c^2}{8M^2E} + \frac{l_c^2\left[l_c^2 + 8M^2(m_0^2 - 4E^2)\right]}{256M^5E^3}\,x + O(x^2), \tag{99}$$

$$\mathcal{I}_3 \equiv \int_0^{l_c} \frac{l^3}{\sqrt{R_0}}\,dl = \frac{2X^{3/2} - \sqrt{R_{0c}}(2X + Yl_c^2)}{3Y^2}$$
$$= \frac{l_c^4}{16M^2E} + \frac{l_c^4\left[l_c^2 + 6M^2(m_0^2 - 4E^2)\right]}{384M^5E^3}\,x + O(x^2), \tag{100}$$

$$\mathcal{I}_4 \equiv \int_0^{l_c} l\sqrt{R_0}\,dl = \frac{X^{3/2} - R_{0c}^{3/2}}{3Y}$$
$$= 2M^2El_c^2 + \frac{l_c^2\left[l_c^2 + 8M^2(m_0^2 - 4E^2)\right]}{16EM}\,x + O(x^2). \tag{101}$$

Substituting these expansions into the general expressions (45)-(50) for the absorption part, we obtain the following near-horizon expansions for the covariant components of the particle current and the stress-energy tensor:

$$J_t^H = -\frac{\pi m_0 A}{4M^2}\left(\langle l_c^2\rangle + \langle \frac{l_c^2\left(l_c^2 + 8M^2\left(m_0^2 - 4E^2\right)\right)}{32E^2M^3}\rangle x + O(x^2)\right), \tag{102}$$

$$J_r^H = \frac{\pi m_0 A}{2Mx}(1 - H_0)\left(\langle l_c^2\rangle - \langle \frac{l_c^2\left(16E^2M^2(1 + 2H_1M) + H_0M^2(l_c^2 + 8M^2(m_0^2 - 2E^2))\right)}{32E^2(1 - H_0)M^3}\rangle x + O(x^2)\right), \tag{103}$$

CPC Accepted

$$T^H_{tt} = \frac{\pi m_0 A}{4M^2}\left(\langle E l_c^2\rangle + \langle \frac{l_c^2\left(l_c^2+8M^2\left(m_0^2-4E^2\right)\right)}{32EM^3}\rangle x + O(x^2)\right), \tag{104}$$

$$T^H_{tr} = -\frac{\pi m_0 A}{2Mx}(1-H_0)\left(\langle E l_c^2\rangle - \langle \frac{l_c^2\left(16E^2M^2(1+2H_1M)+H_0M^2(l_c^2+8M^2(m_0^2-2E^2))\right)}{32E(1-H_0)M^3}\rangle x + O(x^2)\right), \tag{105}$$

$$T^H_{rr} = \frac{\pi m_0 A(1-H_0)^2}{x^2}\left(\langle E l_c^2\rangle - \langle \frac{l_c^2\left(8M^2\left(8E^2H_1M+(H_0+1)m_0^2\right)+(H_0+1)l_c^2\right)}{32E(1-H_0)M^3}\rangle x + O(x^2)\right), \tag{106}$$

$$T^H_{\theta\theta} = \frac{\pi m_0 A}{16M^2}\left(\langle \frac{l_c^4}{E}\rangle + \langle \frac{l_c^4\left(6M^2\left(m_0^2-4E^2\right)+l_c^2\right)}{24E^3M^3}\rangle x + O(x^2)\right). \tag{107}$$

Although the individual components J^H_r, T^H_{tr} and T^H_{rr} diverge as x^{-1} or x^{-2}, physical observables constructed from them remain finite at the horizon. The particle number density $n_H = \sqrt{-g_{\mu\nu}J^\mu_H J^\nu_H}$ is found to be

$$n_H = \frac{\pi m_0 A}{8\sqrt{2}M^3}\sqrt{\langle l_c^2\rangle\langle \frac{l_c^2(l_c^2+8m_0^2M^2)}{E^2}\rangle} + O(x), \tag{108}$$

where the leading term is independent of H_0 and H_1. Diagonalizing the mixed stress-energy tensor $T^\mu_{\ \nu}$ on the horizon gives the energy density and pressures, given to

$$\rho^H = \frac{\pi m_0 A}{192M^4}\left(3f_2 + 2\sqrt{3}\sqrt{f_1 f_3}\right) + O(x), \tag{109}$$

$$p^H_{\rm rad} = \frac{\pi m_0 A}{192M^4}\left(-3f_2 + 2\sqrt{3}\sqrt{f_1 f_3}\right) + O(x), \tag{110}$$

$$p^H_{\rm tan} = T^\theta_{\ \theta} = \frac{\pi m_0 A}{64M^4}\langle \frac{l_c^4}{E}\rangle + O(x), \tag{111}$$

where

$$f_1 = \langle E l_c^2\rangle, \quad f_2 = \langle \frac{l_c^2(l_c^2+8m_0^2M^2)}{E}\rangle,$$
$$f_3 = \langle \frac{l_c^2(l_c^4+12l_c^2m_0^2M^2+48m_0^4M^4)}{E^3}\rangle. \tag{112}$$

All three quantities are manifestly coordinate independent at leading order.

Finally, evaluating the accretion rates $\dot{n} = -4\pi r^2 J^r$ and $\dot{E} = -4\pi r^2 T_t^{\ r}$ at the horizon, we obtain the exact constants

$$\dot{n} = 4\pi^2 m_0 A\langle l_c^2\rangle, \tag{113}$$

$$\dot{E} = 4\pi^2 m_0 A\langle E l_c^2\rangle, \tag{114}$$

which are free of any coordinate artifacts and coincide with the values obtained by integrating the absorption part at any radius.

The above results confirm that, despite the strong coordinate dependence of the individual tensor components near the horizon, the physical properties of the accreting Vlasov gas — density, pressure, and accretion rates — are well defined and invariant.

X. THE ASYMPTOTIC RESULTS OF MAXWELL–JÜTTNER DISTRIBUTION AND THE ACCRETION RATE OF THERMODYNAMIC ENTROPY

In this section we specialize the general expressions obtained in the preceding sections to the Maxwell–Jüttner distribution, which describes a classical relativistic gas in thermal equilibrium. For this case the statistical parameter ε in the distribution function (33) is set to zero and the chemical potential μ is taken to vanish, so that $f = A\delta(P_0 - m_0)e^{-\epsilon z}$, where we have introduce the dimensionless energy $\epsilon = \frac{E}{m_0}$ and the dimensionless inverse temperature $z \equiv \frac{m_0}{k_{\rm B}T}$.

At large distances the geometry is flat and the gas is isotropic. The leading contributions to the particle current density and the stress-energy tensor are given by the scattering part, whose asymptotic expressions have been derived in Sec. VIII. The following integrals are useful

$$\langle \sqrt{\Delta}E\rangle = m_0^3\int_1^\infty \sqrt{\epsilon^2-1}\,\epsilon\,\mathrm{e}^{-z\epsilon}\,d\epsilon = m_0^3\frac{K_2(z)}{z}, \tag{115}$$

$$\langle \sqrt{\Delta}E^2\rangle = m_0^4\int_1^\infty \sqrt{\epsilon^2-1}\,\epsilon^2\,\mathrm{e}^{-z\epsilon}\,d\epsilon = m_0^4\left(\frac{K_1(z)}{z} + 3\frac{K_2(z)}{z^2}\right), \tag{116}$$

CPC Accepted

$$\langle \Delta^{3/2} \rangle = m_0^4 \int_1^\infty (\epsilon^2 - 1)^{3/2} \, \mathrm{e}^{-z\epsilon} \, d\epsilon = m_0^4 \cdot 3 \frac{K_2(z)}{z^2}, \tag{117}$$

where $K_1(z)$ and $K_2(z)$ are the Bessel functions of the first kind and second kind. Using these integrals, one can easily obtain

$$n_\infty = 4\pi A m_0^4 \frac{K_2(z)}{z}, \tag{118}$$

$$\rho_\infty = 4\pi A m_0^5 \left(\frac{K_1(z)}{z} + 3\frac{K_2(z)}{z^2} \right), \tag{119}$$

$$p_\infty = 4\pi A m_0^5 \frac{K_2(z)}{z^2}. \tag{120}$$

One verifies that the ideal gas equation of state $p_\infty = n_\infty k_\mathrm{B} T$ holds identically, which shows the gas behaves exactly as an isotropic perfect fluid at infinity. The average energy of a classical particle at temperature T is

$$\bar{E} = \frac{\rho_\infty}{n_\infty} = m_0 \left(\frac{K_1(z)}{K_2(z)} + \frac{3}{z} \right). \tag{121}$$

In the non-relativistic limit $z \to \infty$, this value approaches

$$\bar{E} = m_0 \left(1 + \frac{3}{2z} \right) = m_0 + \frac{3}{2} k_B T, \tag{122}$$

where we have used the limits $\lim\limits_{z\to\infty} \frac{K_1(z)}{K_2(z)} \approx 1 - \frac{3}{2}z$. The first term in the above expression (122) denotes the rest energy $m_0 c^2$ (here $c = 1$), and the second term $\frac{3}{2}k_B T$ corresponds to the translational kinetic energy arising from the temperature T, which is none other than the classical Maxwell–Boltzmann result.

On the horizon the absorption part dominates and the relevant physical quantities are given by the expressions (108)–(111) together with the definitions of f_1, f_2, f_3. They are complicated expressions. However, similer to the reference [11], one can obtain simpler relevant expressions in the low-temperature limit $z \to \infty$. Let's introduce the dimensionless variables $y = z(\epsilon - 1)$. Then $\epsilon = 1 + y/z$, $\mathrm{d}\epsilon = \mathrm{d}y/z$, and the exponential factor becomes $\mathrm{e}^{-z\epsilon} = \mathrm{e}^{-z}\mathrm{e}^{-y}$. Any average $\langle Q(E) \rangle = \int_{m_0}^\infty Q(E) \mathrm{e}^{-E/k_\mathrm{B}T} dE$ transforms to

$$\langle Q \rangle = m_0 \mathrm{e}^{-z} \int_0^\infty Q\left(m_0 \left(1 + \frac{y}{z} \right) \right) \mathrm{e}^{-y} \frac{\mathrm{d}y}{z}.$$

In the limit $z \to \infty$, the following expressions are obtained:

$$l_c^2 \approx \frac{E l_c^2}{m_0} \approx 16 m_0^2 M^2, \tag{123}$$

$$\frac{l_c^2 (l_c^2 + 8m_0^2 M^2)}{E^2} \approx m_0 \frac{l_c^2 (l_c^2 + 8m_0^2 M^2)}{E} \approx 384 m_0^2 M^4, \tag{124}$$

$$\frac{l_c^2 (l_c^4 + 12 l_c^2 m_0^2 M^2 + 48 m_0^4 M^4)}{E^3} \approx 7936 m_0^3 M^6, \tag{125}$$

$$\frac{l_c^4}{E^2} \approx 256 m_0^3 M^4. \tag{126}$$

Since the leading terms in these expressions are constant, the averages of these quantities are proportional to $\frac{e^{-z}}{z}$; for example,

$$\langle l_c^2 \rangle \approx m_0 \frac{e^{-z}}{z} \int_0^\infty 16 m_0^2 M^2 e^{-y} dy = 16 m_0^3 M^2 \frac{e^{-z}}{z}. \tag{127}$$

After performing similar mathematical calculations, we obtain

$$n_H = 4\sqrt{3}\pi m_0^4 A \frac{e^{-z}}{z}, \tag{128}$$

$$\rho_H = \frac{2}{3}(9 + \sqrt{93})\pi m_0^5 A \frac{e^{-z}}{z}, \tag{129}$$

$$p_{\mathrm{rad}}^H = \frac{2}{3}(-9 + \sqrt{93})\pi m_0^5 A \frac{e^{-z}}{z}, \tag{130}$$

$$p_{\mathrm{tan}}^H = 4\pi m_0^5 A \frac{e^{-z}}{z}. \tag{131}$$

The ratios to the particle density n_H therefore remain finite in the limit $z \to \infty$

$$\frac{\rho_H}{n_H} = \frac{m_0}{2\sqrt{3}} \left(3 + \sqrt{\frac{31}{3}} \right), \tag{132}$$

$$\frac{p_{\mathrm{rad}}^H}{n_H} = \frac{m_0}{2\sqrt{3}} \left(-3 + \sqrt{\frac{31}{3}} \right), \tag{133}$$

$$\frac{p_{\mathrm{tan}}^H}{n_H} = \frac{m_0}{\sqrt{3}}, \tag{134}$$

and the compression ratio $\frac{n_H}{n_\infty}$ is

CPC Accepted

$$\lim_{z\to\infty}\frac{1}{\sqrt{z}}\frac{n_H}{n_\infty}=\lim_{z\to\infty}\frac{\sqrt{3}}{\sqrt{z}}\frac{e^{-z}}{K_2(z)}=\sqrt{\frac{6}{\pi}}. \tag{135}$$

For finite values of z, numerical integration can be employed; the results are shown in Fig. 1. The accretion rates are

$$\dot{n}\approx\frac{\dot{E}}{m_0}\approx 64\pi^2 m_0^5 A M^2\frac{e^{-z}}{z}, \tag{136}$$

and the mass accretion rate $\dot{M}=m_0\dot{n}$ is approximated as

$$\lim_{z\to\infty}\frac{1}{\sqrt{z}}\frac{\dot{M}}{n_\infty}=\lim_{z\to\infty}\frac{16\pi m_0 M^2}{\sqrt{z}}\frac{e^{-z}}{K_2(z)}=16\sqrt{2\pi}m_0M^2. \tag{137}$$

These asymptotic results coincide with those obtained by Rioseco and Sarbach [11] in their low-temperature analysis, thereby confirming the consistency of our horizon expansions.

This quantity can be computed more precisely. The average energy of a single particle falling into the black hole is defined as

$$\bar{E}=\frac{\dot{E}}{\dot{n}}=\frac{\langle E l_c^2\rangle}{\langle l_c^2\rangle}. \tag{138}$$

In the classical limit $z\to\infty$, expanding to first order in $1/z$, we obtain

$$\bar{E}\approx\frac{1+\frac{5}{z}}{1+\frac{4}{z}}\approx m_0\left(1+\frac{1}{z}\right)=m_0+k_BT, \tag{139}$$

where the first term denotes the rest energy, and the second term denotes the translational kinetic energy associated with the temperature T, which is smaller than $\frac{3}{2}k_BT$. This implies that particles captured by the black hole are subject to angular-momentum selection. Particles with higher energies are more likely to possess large angular momenta, making them more likely to be scattered back to infinity by the centrifugal barrier. Consequently, the energy spectrum of the captured particles is truncated and softened, and their mean energy is below the overall average.

Moreover, we now consider the entropy accretion rate. The entropy flux through a spherical surface of arbitrary radius can be defined as

$$\dot{S}=4\pi r^2 k_B\int_{abs} f(x,p)\ln f(x,p)\,p^r\,\mathrm{dvol}_x(p). \tag{140}$$

Substituting the expression $f=A\delta(P_0-m_0)e^{-\frac{E}{k_BT}}$ yields

$$\begin{aligned}\dot{S}&=-k_B\ln A\left(-4\pi\int_{abs}f(x,p)p^r\,\mathrm{dvol}_x(p)\right)\\&\quad+\frac{1}{T}\left(-4\pi\int_{abs}Ef(x,p)p^r\,\mathrm{dvol}_x(p)\right)\\&=-k_B\ln A\,\dot{n}+\frac{\dot{E}}{T}.\end{aligned} \tag{141}$$

The specific entropy is defined as $\sigma_{abs}=\frac{\dot{S}}{\dot{n}}$, where

$$\sigma_{abs}=-k_B\ln A+\frac{\bar{E}}{T}=k_B(-\ln A+z+1). \tag{142}$$

At infinity, the system is characterized by a Maxwell–Jüttner distribution, and the specific entropy is given by $\sigma=k_B(-\ln A+z+\frac{5}{2})$. This indicates that the entropy per particle of the accreted particles is lower than the global average by $\frac{3}{2}k_B$.

XI. NUMERICAL RESULTS

A. Particle current density and particle density

We perform the numerical calculation using Wolfram Mathematica. Without loss of generality, we choose $M=1$ and $\mu=0$. Fig. 2 shows the numerical results for J_t and J_r, where J_r depends on the metric form and is calculated using three different metrics. The three coordinate systems exhibit different asymptotic behaviors. When $h=0$, J_r diverges at the horizon and approaches zero at infinity. When $h=1$, the values of J_r at the horizon and at infinity are finite, as given by Eq. (103) and Eq. (82), respectively. However, the particle density is coordinate independent, as shown in Fig. 3. The reason why the coordinate dependence of J_r does not affect physical quantities can be seen directly from Eqs. (45) and (46). Since $g^{rr}=b^2$ and $g^{tr}=-h$ (using $a^2b^2+h^2=1$), the contravariant component is

$$J^r=b^2J_r-hJ_t=\pm\frac{2\pi m_0 A}{r^2}\iint\frac{l}{e^{(E-\mu)/k_BT}+\epsilon}\,dE\,dl, \tag{143}$$

where the terms proportional to $hE/\sqrt{R_0}$ cancel identically. Thus, r^2J^r remains the same function of r, and $\dot{n}=-4\pi r^2J^r$ is manifestly invariant.

The numerical results for $\frac{n_H}{n_\infty}$ for the Maxwell-Jüttner distribution are shown in Fig. 3. The values of $\frac{n_H}{n_\infty}$ obtained for the other two distributions are also very similar, as shown in Table 1. This similarity can be explained

CPC Accepted

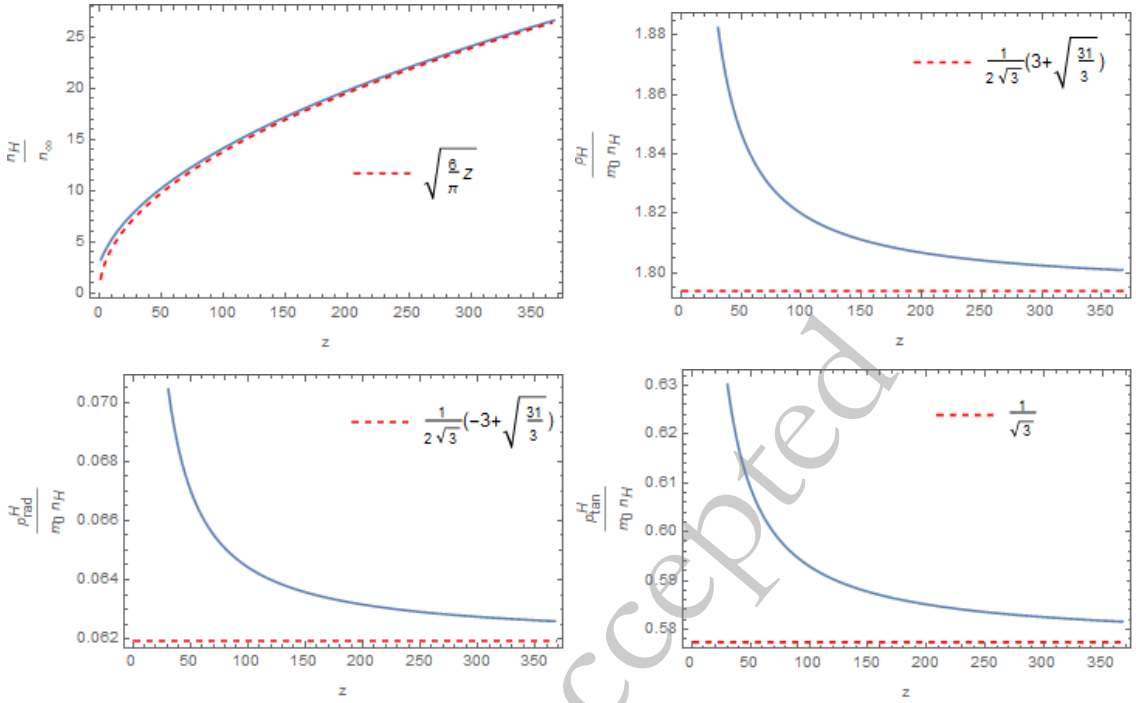


Fig. 1. (color online) The numerical values of $\frac{n_H}{n_\infty}, \frac{\rho_H}{n_H}, \frac{p^H_{\rm rad}}{n_H}, \frac{p^H_{\rm rad}}{n_H}$ are given for finite z.

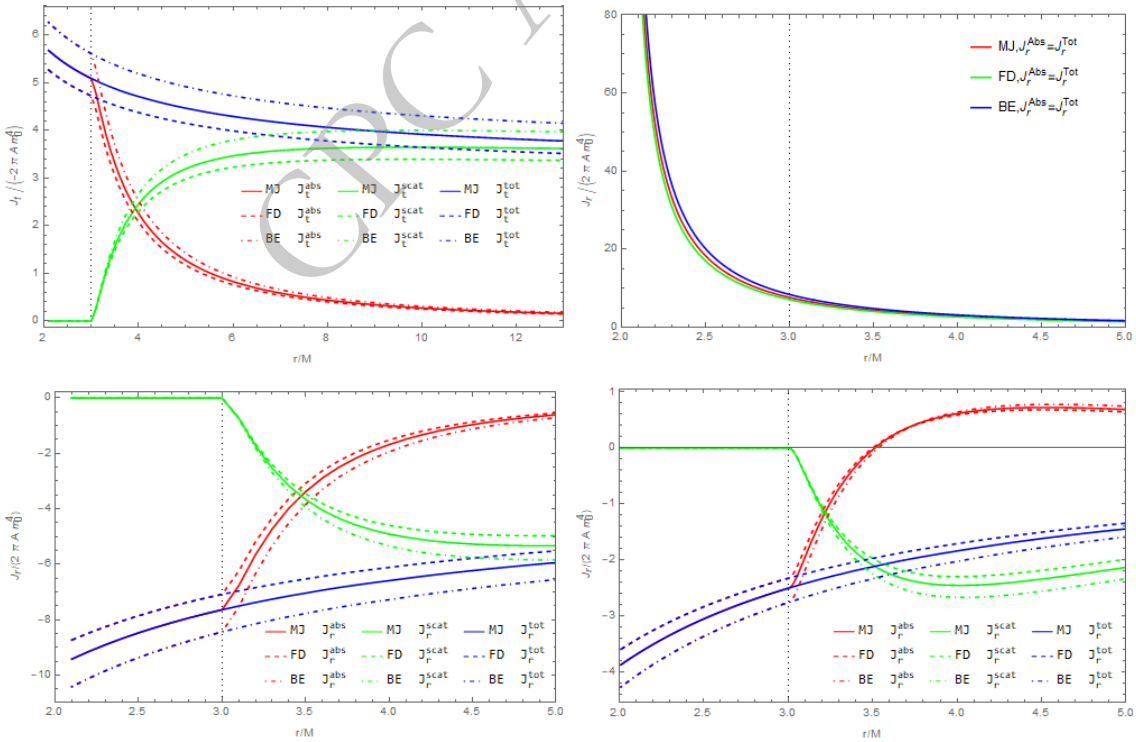


Fig. 2. Numerical values of J_t and J_r for $z=1$. The metric used for the image in the right panel of the first row is $h=0$. At this point, the scattered components of the incident and outgoing branches cancel each other, leaving only the absorbing component. The image in the left panel of the second row uses the metric $h=1$, and the image in the right panel of the second row uses the metric $h=2/r$.

as follows: the integral has the form

$$\langle \sqrt{\Delta E}\rangle = m_0^3 \int_1^\infty \sqrt{\epsilon^2-1}\,\epsilon\,\frac{1}{e^{z\epsilon}+\varepsilon}\,d\epsilon, \qquad (144)$$

where the parameter ε has only a limited influence on the integral, and this effect diminishes further as z increases. For this reason, it is difficult to distinguish the different distributions from the plot of $\frac{n_H}{n_\infty}$. The near-independence

CPC Accepted

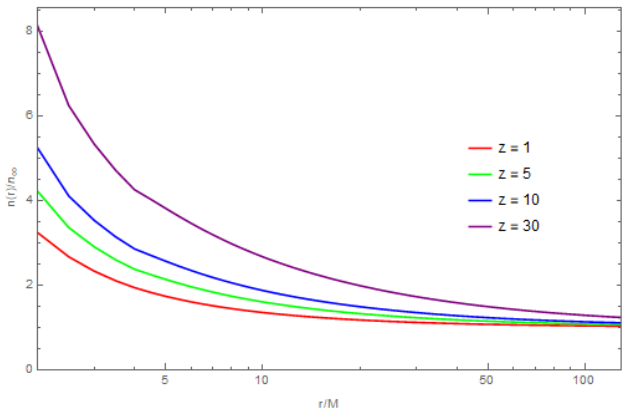


Fig. 3. (color online) The behavior of the compression ratio $n(r)/n_\infty$ as a function of r/M for different temperatures in Maxwell-Jüttner statistics.

Table 1. Numerical results for $\frac{n_H}{n_\infty}$ are presented for three different statistics. The chemical potential is set to $\mu = 0$.

distribution	z=1	z=5	z=10	z=30
$\varepsilon = 0$	3.24405	4.22358	5.24868	8.13214
$\varepsilon = 1$	3.22868	4.22151	5.24866	8.13214
$\varepsilon = -1$	3.26997	4.22567	5.24871	8.13214

of n_H/n_∞ on the statistical parameter ϵ has a simple physical origin. The distribution function depends on ϵ only through the denominator $e^{z\epsilon-\tilde{\mu}}+\epsilon$, so the quantum-statistical correction relative to the classical case is of order $\epsilon e^{-(z\epsilon-\tilde{\mu})}$. This correction is appreciable only in the low-energy region $z\epsilon \sim \tilde{\mu}$. By contrast, the accreted particles originate from the high-energy tail selected by $l < l_c(E)$ and by the factor $e^{-z(\epsilon-1)}$, where $e^{z\epsilon-\tilde{\mu}} \gg 1$ and the ± 1 term is negligible. Moreover, low-energy particles carry small angular momenta and are easily scattered by the centrifugal barrier, so they contribute little to n_H. Hence, all three statistics yield nearly identical accretion rates. As z increases, the exponential cutoff further narrows the accretion window, and the residual correction, which is of order e^{-z}, decreases. This explains why the differences among the three distributions diminish with increasing z.

B. Energy density, radial and tangential pressures

The components of the energy-momentum tensor $T_{\mu\nu}(\mu, \nu = t, r)$ are plotted in Fig. 4. By diagonalizing $T^{\mu}{}_{\nu}$, we obtain the coordinate-independent physical quantities $\frac{\rho}{n}$, $\frac{p_{\rm rad}}{n}$, and $\frac{p_{\rm tan}}{n}$, which are plotted for the Maxwell-Jüttner distribution in Fig. 5. These results are consistent with Ref. [12], showing that $p_{\rm rad} = p_{\rm tan}$ at infinity. However, as r/M decreases, $p_{\rm rad}$ gradually becomes smaller than $p_{\rm tan}$.

In Table 2, we present the numerical results for $\frac{\rho}{nm_0}$, $\frac{p_{\rm rad}}{nm_0}$, and $\frac{p_{\rm tan}}{nm_0}$ in the near-horizon and asymptotic-infinity limits for three different distributions. The table shows that the differences among these results are very small. Therefore, the numerical results for $\frac{\rho}{nm_0}$, $\frac{p_{\rm rad}}{nm_0}$, and $\frac{p_{\rm tan}}{nm_0}$ for the other two distributions will be very similar to those shown in Figure 5, and we do not plot them separately here. The results in Table 2 were also used to examine the asymptotic behavior in Figure 5.

XII. CONCLUSION AND DISCUSSION

In this work, we systematically investigated the coordinate dependence of stationary, spherically symmetric accretion of a relativistic Vlasov gas onto a Schwarzschild black hole. Working within the most general stationary metric that admits off-diagonal g_{tr} components, we derived the equations of motion, constructed action-angle variables, and obtained exact integral expressions for the particle current density and the stress-energy tensor. Our analysis covers three distinct statistical distributions—Fermi–Dirac, Maxwell–Jüttner, and Bose–Einstein—and includes both asymptotic expansions (at infinity and near the horizon) and full numerical integrations at finite radii. The central result is that, although the individual covariant components of J_μ and $T_{\mu\nu}$ depend explicitly on the chosen coordinate system, all physically observable quantities—namely, the particle number density n, energy density ρ, radial and tangential pressures $p_{\rm rad}$ and $p_{\rm tan}$, and the accretion rates $\dot{m}$ and $\dot{E}$—are manifestly coordinate invariant. This invariance is achieved through appropriate combinations of tensor components and is guaranteed by the identity $a^2b^2 + h^2 = 1$, which holds for all coordinate representations considered.

A key physical insight emerging from our study is the role of angular momentum in filtering the accreted particles. At infinity, the gas is isotropic and obeys the classical ideal-gas equation of state, with mean energy $m_0 + \frac{3}{2}k_BT$. However, particles captured by the black hole have, on average, lower energy: in the nonrelativistic limit, their mean energy is $m_0 + k_BT$. This reduction occurs because high-energy particles tend to carry large angular momenta, making them more likely to be scattered by the centrifugal barrier than absorbed. Consequently, the specific entropy of the accreted particles is lower than the global average by $\frac{3}{2}k_B$, indicating that the accretion process effectively selects the lower-entropy, lower-energy portion of the phase-space distribution. These findings highlight that black hole accretion in the kinetic regime is not merely a passive capture process but involves a dynamical filtering mechanism that modifies the thermodynamic properties of the infalling matter.

From a methodological standpoint, our formulation does not rely on any particular coordinate system, thereby providing a unified framework that can be readily exten-

CPC Accepted

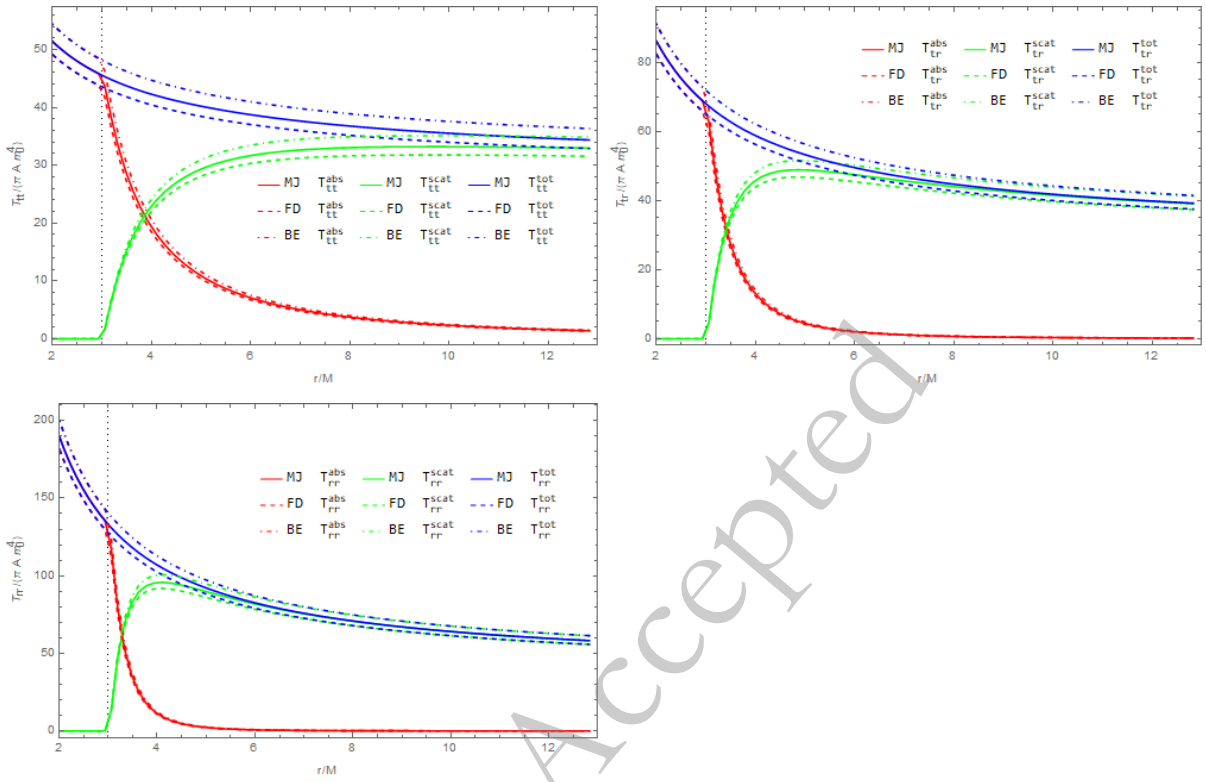


Fig. 4. (color online) Numerical values of T_{tt}, T_{tr}, and T_{rr} for $z=1$. We set the metric $h=1$.

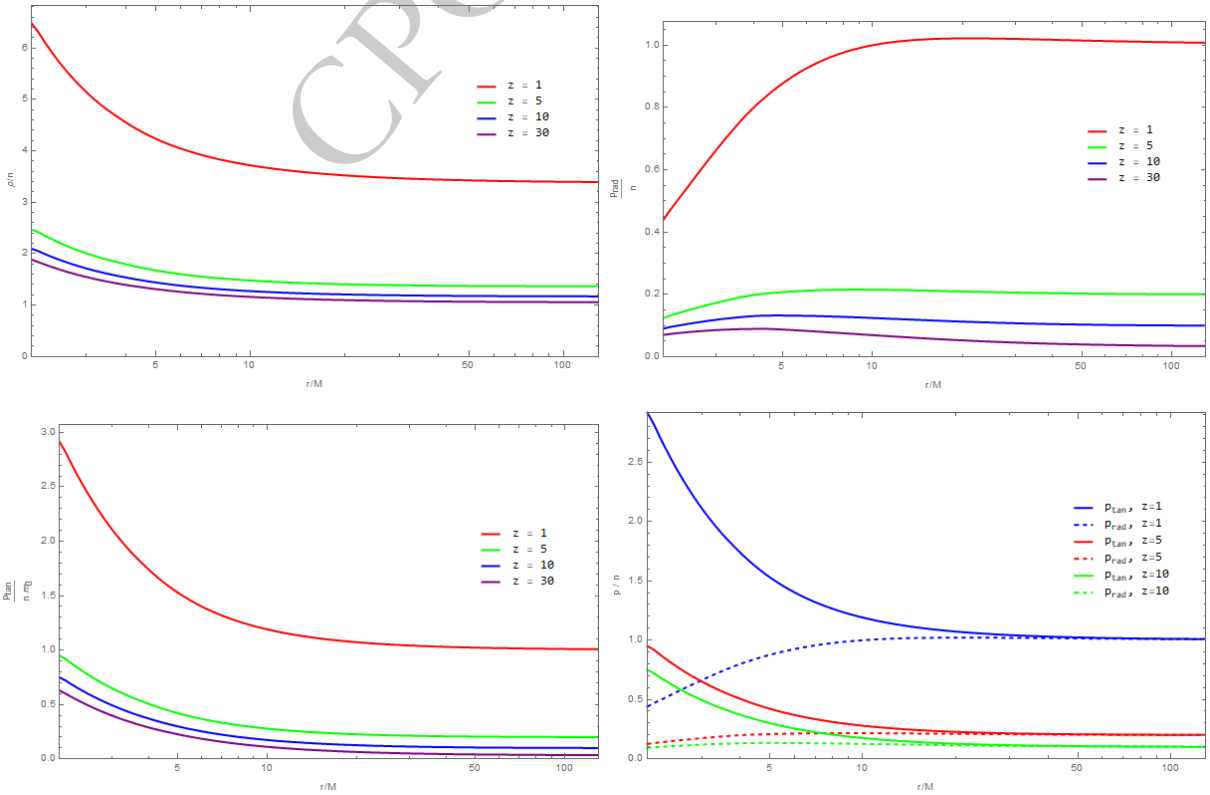


Fig. 5. (color online) The numerical values of $\frac{\rho}{nm_0}$, $\frac{P_{\rm rad}}{nm_0}$, and $\frac{P_{\tan}}{nm_0}$ as functions of r/M for the Maxwell-Jüttner distribution.

CPC Accepted

Table 2. The asymptotic numerical results for $\frac{\rho}{nm_0}$, $\frac{p_{\rm rad}}{nm_0}$, and $\frac{p_{\tan}}{nm_0}$ under three different statistics.

		$z=1$		$z=5$		$z=10$		$z=30$	
		$r/M=2$	$r/M=\infty$	$r/M=2$	$r/M=\infty$	$r/M=2$	$r/M=\infty$	$r/M=2$	$r/M=\infty$
$\frac{\rho}{nm_0}$	$\varepsilon=0$	6.48658	3.37044	2.4693	1.36185	2.09571	1.16699	1.88471	1.05202
	$\varepsilon=1$	6.68286	3.46204	2.47024	1.36224	2.09571	1.16699	1.88471	1.05202
	$\varepsilon=-1$	6.22378	3.25017	2.46836	1.36145	2.09571	1.16699	1.88471	1.05202
$\frac{p_{\rm rad}}{nm_0}$	$\varepsilon=0$	0.439051	1	0.124059	0.2	0.0906328	0.1	0.0706736	0.0333333
	$\varepsilon=1$	0.454003	1.03457	0.124141	0.200202	0.0906331	0.100001	0.0706736	0.0333333
	$\varepsilon=-1$	0.418946	0.954133	0.123977	0.199797	0.0906325	0.0999993	0.0706736	0.0333333
$\frac{p_{\tan}}{nm_0}$	$\varepsilon=0$	2.91865	1	0.950425	0.2	0.749912	0.1	0.630925	0.0333333
	$\varepsilon=1$	3.01316	1.03457	0.950929	0.200202	0.749914	0.100001	0.630925	0.0333333
	$\varepsilon=-1$	2.79163	0.954133	0.949919	0.199797	0.74991	0.0999993	0.630925	0.0333333

CPC Accepted

ded to other black hole spacetimes, such as Reissner–Nordström or Kerr, and even to modified theories of gravity with asymptotically flat solutions. The use of action-angle variables and the explicit construction of the invariant phase-space volume element ensure that the Vlasov equation is solved consistently and that the resulting distribution function remains a steady-state solution throughout the spacetime. The asymptotic expansions at the horizon and at infinity, together with the numerical results at finite radii, confirm the robustness of our conclusions across all regimes. We have also shown that the differences among the three quantum statistics become negligible at low temperatures, as expected, because the classical Maxwell–Jüttner limit is recovered.

In summary, our work establishes that the accretion of a collisionless kinetic gas onto a Schwarzschild black hole can be described in a fully coordinate-independent manner, with unambiguous definitions of all physical observables. The results not only resolve potential ambiguities arising from different metric representations but also provide a solid foundation for future investigations of more complex accretion scenarios, including rotating black holes, charged black holes, and systems with external perturbations. The entropy reduction and energy-filtering effects identified here may have important implications for the thermodynamics of black hole growth and the evolution of particle distributions in strong gravitational fields.

References

[1] H. Bondi, Mon. Not. R. Astron. Soc. **112**, 195 (1952)
[2] F. C. Michel, Astrophys. Space Sci. **15**, 153 (1972)
[3] K. Akiyama *et al*. (Event Horizon Telescope Collaboration), Astrophys. J. Lett. **875**, L1 (2019)
[4] K. Akiyama *et al*. (Event Horizon Telescope Collaboration), Astrophys. J. Lett. **930**, L12 (2022)
[5] J. L. Synge, Trans. R. Soc. Can. **28**, 127 (1934)
[6] J. Ehlers, General relativity and kinetic theory, in *General Relativity and Cosmology*, edited by R. K. Sachs (Academic Press, New York, 1971), pp. 1–70.
[7] O. Sarbach and T. Zannias, AIP Conf. Proc. **1548**, 134 (2013)
[8] O. Sarbach and T. Zannias, Class. Quantum Grav. **31**, 085013 (2014)
[9] R. O. Acuña-Cárdenas, C. Gabarrete, and O. Sarbach, Gen. Relativ. Gravit. **54**, 23 (2022)
[10] H. Andréasson, Living Rev. Relativ. **14**, 4 (2011)
[11] P. Rioseco and O. Sarbach, Class. Quantum Grav. **34**, 095007 (2017)
[12] P. Rioseco and O. Sarbach, J. Phys. Conf. Ser. **831**, 012009 (2017)
[13] A. Cieślik and P. Mach, Class. Quantum Grav. **39**, 225003 (2022)
[14] A. Cieślik, E. Hackmann, and P. Mach, Phys. Rev. D **108**, 024056 (2023)
[15] P. Mach and A. Odrzywołek, Phys. Rev. Lett. **126**, 101104 (2021)
[16] P. Mach and A. Odrzywołek, Phys. Rev. D **103**, 024044 (2021)
[17] P. Mach and A. Odrzywołek, Acta Phys. Pol. B Proc. Suppl. **15**, 1 (2022)
[18] A. Cieślik and P. Mach, Phys. Rev. D **102**, 024032 (2020)
[19] P. Li, J. Yang, and S. Xu, Phys. Lett. B **866**, 139555 (2025)
[20] Y. Liu and H. Zhang, Accretion of a Plasma Vlasov Gas onto a Reissner–Nordström Black Hole, arXiv: 2606.25425 (2026).
[21] A. Gamboa, C. Gabarrete, P. Domínguez-Fernández, D. Núñez, and O. Sarbach, Phys. Rev. D **104**, 083001 (2021)
[22] J. Liao and D. Liu, Astrophys. Space Sci. **367**, 109 (2022)
[23] Z. Cai and R. Yang, Phys. Dark Universe **42**, 101292 (2023)
[24] M. Momennia and O. Sarbach, Class. Quantum Grav. **42**, 155020 (2025)
[25] X. X. Zhang and Y. H. Jiang, Chinese Phys. C **49**, 025101

(2025)
[26] C. Gabarrete and O. Sarbach, Acta Phys. Pol. B Proc. Suppl. **15**, 1 (2022)
[27] C. Gabarrete and O. Sarbach, Class. Quantum Grav. **40**, 055012 (2023)
[28] S. L. Shapiro, Phys. Rev. D **108**, 083037 (2023)
[29] P. Mach, M. Momennia, and O. Sarbach, Phys. Rev. D **113**, 044068 (2026)
[30] P. Mach, M. Momennia, and O. Sarbach, Phys. Rev. D **113**, L041505 (2026)
[31] P. Li, Y. Liu, and X. Zhai, Phys. Rev. D **108**, 124022 (2023)
[32] Y. Liu, A discussion on the symmetry of relativistic Vlasov gas and its accretion in Kerr–Newman black hole, arXiv: 2506.08341 (2025).
[33] G. Khan and P. Mach, Phys. Rev. D **111**, 084057 (2025)
[34] M. Luepker, Y. Yuan, and A. Y. Chen, Stable Collisionless Tori Around Kerr Black Holes, arXiv: 2508.09077 (2025).
[35] P. Rioseco and O. Sarbach, Phys. Rev. D **98**, 124024 (2018)
[36] P. Rioseco and O. Sarbach, Commun. Math. Phys. **405**, 105 (2024)
[37] E. Tejeda, P. A. Taylor, and J. C. Miller, Mon. Not. R. Astron. Soc. **429**, 925 (2013)
[38] Z. Bakun, A. Lukanty, A. Untilova, A. Cieślik, and P. Mach, Class. Quantum Grav. **42**, 015004 (2025)
[39] A. Aguayo-Ortiz, E. Tejeda, O. Sarbach, and D. Lopez-Camara, Mon. Not. R. Astron. Soc. **504**, 5039 (2021)
[40] P. Pani, E. Berti, and L. Gualtieri, Phys. Rev. Lett. **110**, 241103 (2013)
[41] L. I. Petrich, S. L. Shapiro, and S. A. Teukolsky, Phys. Rev. Lett. **60**, 1781 (1988)
[42] P. Mach, A. Cieślik, and A. Odrzywołek, Phys. Rev. D **108**, 124057 (2023)
[43] A. Cieślik, P. Mach, and A. Odrzywołek, Phys. Rev. D **110**, 084014 (2024)
[44] Luciano Rezzolla, Olindo Zanotti, Relativistic Hydrodynamics, Oxford University Press, 09 (2013).
[45] F. Jüttner, Annal. Phys. **339**, 856 (1911)
[46] F. Jüttner, Ann. Phys. **35**, 145 (1911)
[47] Ping Li, Jun Cheng, and Jiang-he Yang, Chin. Phys. C **50**, 075103 (2026)
[48] P. S. Letelier, Phys. Rev. D **22**, 807 (1980)
[49] Y. Liu and X. Zhang, Phys. Rev. D **111**, 044056 (2025)
[50] X. Wu and X. Zhang, Universe **8**, 604 (2022)

CPC Accepted